JOURNAL OF SOLID STATE CHEMISTRY 68, 143–152 (1987)

$BaLa_4Cu_5O_{13+\delta}$, an Oxygen-Deficient Perovskite Built Up from Corner-Sharing CuO_6 Octahedra and CuO_5 Pyramids

C. MICHEL, L. ER RAKHO, AND M. HERVIEU

Laboratoire de Cristallographie, Chimie et Physique des Solides, U.A. 251, ISMRa-Université, 14032 Caen Cedex, France

J. PANNETIER

Institut Max Von Laue, Paul Langevin, 156X Centre de Tri, 38042 Grenoble Cedex, France

AND B. RAVEAU

Laboratoire de Cristallographie, Chimie et Physique des Solides, U.A. 251, ISMRa-Université, 14032 Caen Cedex, France

Received July 14, 1986

The structure of an oxygen-deficient perovskite $BaLa_4Cu_5O_{13+\delta}$ has been determined by neutron powder diffraction and high-resolution electron microscopy. It has been resolved in the space group $P4/m$ ($a \sim a_p\sqrt{5}$, $c \sim a_p$). The framework $[Cu_5O_{13}]$ is built up from corner-sharing CuO_5 pyramids and CuO_6 octahedra forming hexagonal tunnels and perovskite cages where the La^{3+} and Ba^{2+} ions are located in an ordered manner. The barium ions are located in the perovskite tunnels whereas the lanthanum ions are located in the hexagonal tunnels. One typical feature of the host lattice $[Cu_5O_{13}]$ deals with the geometry of the hexagonal tunnels which is rather different from the ideal model derived from the stoichiometric perovskite. O–O–O angles are close to 70° (instead of 90°) and O(5)–O(5) distances are close to 3 Å (instead of 3.8 Å). A great number of crystals exhibit a single oxygen-deficient perovskite which can be considered as having the stoichiometry $BaLa_4Cu_5O_{13}$; the excess of oxygen, δ, corresponds to the formation in other crystals of superstructures ($\sim a_p\sqrt{10} \times a_p\sqrt{10} \times a_p$) and of microdomains which are interpreted as the result of a distortion of the $[Cu_5O_{13}]$ matrix induced by the introduction of oxygen in half of the hexagonal tunnels. © 1987 Academic Press, Inc.

Introduction

The ability of copper to take several coordinations—octahedral, square, and pyramidal—and different oxidation states (Cu(II)–Cu(III)) has allowed several oxygen-deficient perovskites and relatives to be synthesized (*1–3*). This behavior of copper is to be compared to that of manganese for which several oxygen-deficient perovskites $CaMnO_{3-x}$ (*4–8*) and $SrMnO_{3-x}$ (*9, 10*) have been isolated. These results are in agreement with the Jahn Teller character of the Cu(II) and Mn(III) ions. The manganese perovskites are characterized by the presence of hexagonal tunnels which result from the ordered elimination of rows of oxygen atoms parallel to the [001] direction of

0022-4596/87 $3.00
Copyright © 1987 by Academic Press, Inc.
All rights of reproduction in any form reserved.

the cubic cell. At the present time, no example of such an ordering of oxygen vacancies was observed in the copper oxides, but in a recent study (*11*) a new oxygen-deficient perovskite $La_4BaCu_5O_{13+\delta}$ was isolated whose parameters ($a \simeq a_p\sqrt{5}$ and $c \simeq a_p$) suggest close relationships with the manganese oxides. The present work deals with the neutron diffraction and high-resolution electron microscopy studies of this oxide in order to understand the ordering of the oxygen vacancies in the perovskite matrix.

Experimental

Synthesis and chemical analysis. This oxide was prepared in air from an appropriate mixture of $BaCO_3$, La_2O_3, and CuO. The mixture was decarbonated at 900°C, ground, then heated at 1000°C for 48 hr, and finally quenched to room temperature.

The oxidation state of copper and consequently the oxygen content were determined by redox back titration using Fe(II) salt and $K_2Cr_2O_7$.

Neutron diffraction. The neutron diffraction pattern at room temperature was collected with the D1A multicollimator diffractometer at the Laue–Langevin Institute (Grenoble) with a wavelength of 1.9570 Å from a germanium monochromator. The powdered sample was inserted in a standard vanadium can ($\phi \sim 10$ mm). The diffractometer has a counter bank with 10 high-pressure He^3 counters covering 60° in 2θ in steps of 6°. The counter bank can be swept through 0° to $2\theta = 160°$ in steps of 0.05°. Structural study was carried out using a profile refinement of diffraction lines program (*12, 13*). The neutron scattering lengths were taken from (*14*): 0.525 (Ba), 0.772 (Cu), 0.824 (La), and 0.580 (O) (all values in femtometers).

Electron microscopy. The microscopy samples were obtained from the polycrystalline sinters by crushing in alcohol, suspending, and depositing onto holey carbon films. The electron diffraction investigation was carried out with a JEOL 120 CX microscope (120 kV), fitted with a side-entry goniometer (±60°). The high-resolution electron microscopy (HREM) images were recorded with a JEM 200 CX fitted with a top-entry goniometer providing ±10° tilt about two axes; the aberration constant of the objective lens was $C_s = 0.8$ mm and the objective aperture radius was 0.47 $Å^{-1}$ in the reciprocal space. Crystals were tilted into a suitable orientation, with [001] parallel to the electron beam and astigmatism was corrected by observing the granularity of the carbon film. Micrographs were recorded at magnifications in the range 550,000–710,000. Simulated images were calculated using the multislice method and computer programs written by Skarnulis *et al.* (*15*).

Results and Discussion

The chemical analysis of the samples showed that the oxygen content of the perovskite phase was sensitive to the method of preparation. For instance, it was observed that the samples prepared in the form of powder were slightly less oxidized ($\delta = 0.16 \pm 0.05$) than those obtained in the form of sintered bars ($\delta \simeq 0.4$) (*11*). However, in both cases the X-ray diffraction analysis showed that a single pure perovskite phase was isolated.

The X-ray powder diffraction study of this oxide had previously shown (*11*) that the metallic atoms were slightly displaced from the ideal position in the cubic perovskite, leading to a tetragonal cell, $a \simeq a_p\sqrt{5}$ and $c \simeq a_p$. The electron diffraction study confirms without any ambiguity that a majority of crystals exhibit a tetragonal symmetry without any reflection condition as shown from the electron diffraction patterns [001] and [100] (Fig. 1).

The consideration of the oxygen content

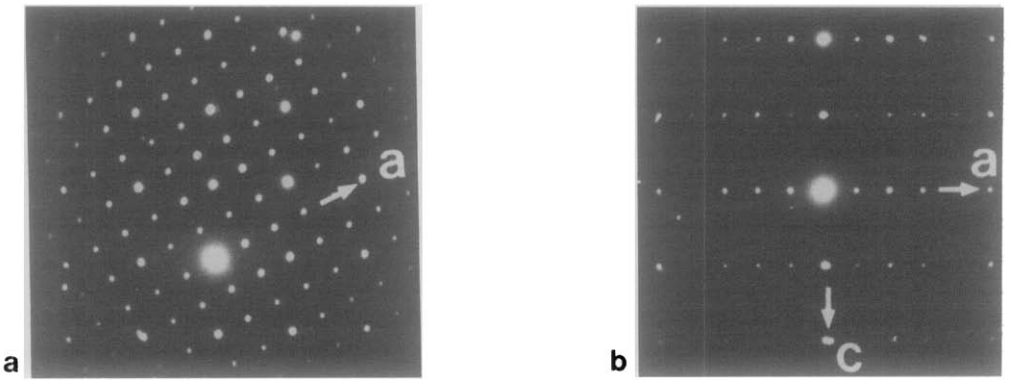

FIG. 1. Electron diffraction patterns. (a) |001|; (b) |100|.

in the oxide $BaLa_4Cu_5O_{13.16}$ suggests two limit possibilities about the ordering of the oxygen vacancies compatible with the cell dimensions. The first hypothesis, which corresponds to the formulation $BaLa_4Cu_5O_{13}$, is characterized by the presence of two oxygen vacancies per cell, whereas the second one, with only one vacancy per cell, has the formulation $BaLa_4Cu_5O_{14}$. A model which can be proposed for $BaLa_4Cu_5O_{13}$ (Fig. 2a) consists of groups of four corner-sharing CuO_5 pyramids linked through CuO_6 octahedra in such a way that each octahedron shares four corners with four pyramids and two corners with two other octahedra, and each pyramid is connected to four other pyramids and one octahedron. The model corresponding to $BaLa_4Cu_5O_{14}$ was previously proposed by Reller and colleagues (*8*) for $CaMnO_{2.8}$ (Fig. 2b): the framework consists of pyramidal files surrounded by octahedral files in such a way that a CuO_5 pyramid shares two corners with two other pyramids and three corners with CuO_6 octahedra, and each octahedron shares four corners with other octahedra and two corners with CuO_5 pyramids. Thus the $BaLa_4Cu_5O_{14}$ model can be deduced from the one of $BaLa_4Cu_5O_{13}$ by introduction of rows of oxygen atoms in one hexagonal tunnel out of two so that the first framework exhibits two hexagonal tunnels and one perovskite tunnel per cell, and the second one exhibits one hexagonal tunnel and three perovskite tunnels per cell.

In order to understand the oxygen nonstoichiometry and especially to determine whether these two structures exist in the form of a mixture of different crystals or of microdomains in the same crystal, neutron diffraction and HREM studies were undertaken successively.

Neutron Diffraction Study

The structure calculations were carried out with powder diffraction data, in the space group $P4/m$ previously used for the X-ray structural study (*11*). In the range $2\theta = 6$–$156°$, 60 diffraction lines were measured corresponding to 182 *hkl*. The refined cell parameters deduced from the neutron diffraction pattern were found to be very close to those calculated from the X-ray dif-

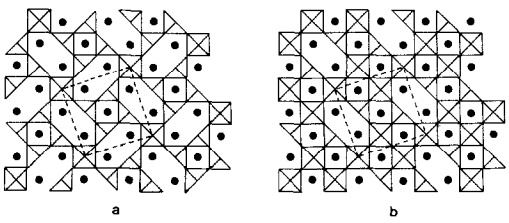

FIG. 2. Ideal projection of the framework on to (001). (a) $BaLa_4Cu_5O_{13}$; (b) $BaLa_4Cu_5O_{14}$.

TABLE I

ATOMIC PARAMETERS OF $BaLa_4Cu_5O_{13.16}$ DETERMINED BY NEUTRON DIFFRACTION (SPACE GROUP $P4/m$)

Atom	Site	x	y	z	B^a (Å^2)
Ba	1(d)	0.5	0.5	0.5	B_{eq} = 0.64(18)
La	4(k)	0.1262(3)	0.2789(4)	0.5	1.02(6)
Cu(1)	1(a)	0	0	0	1.19(10)
Cu(2)	4(j)	0.4154(4)	0.1718(3)	0	0.52(6)
O(1)	1(b)	0	0	0.5	B_{eq} = 1.39(25)
O(2)[b]	2(e)	0	0.5	0	1.0
O(3)	4(j)	0.2697(6)	0.3905(6)	0	1.27(10)
O(4)	4(j)	0.2267(6)	0.0650(6)	0	1.10(7)
O(5)	4(k)	0.4157(6)	0.1559(5)	0.5	1.00(9)

	U_{11}	U_{22}	U_{33}	$U_{12} = U_{13} = U_{23} = 0$
Ba	0.0088(38)	0.0088(38)	0.0070(60)	
O(1)	0.0260(44)	0.0260(44)	0.0007(10)	

[a] B_{eq} values were obtained from $B_{eq} = (4/3)\,\Sigma_i\Sigma_j\,\beta_{ij}a_ia_j$ and the values of anisotropic thermal coefficients from $U_{ij} = (1/2\pi^2)\,\beta_{ij}a_ia_j$ (Å^2).

[b] Partially filled site (τ = 0.06 ± 0.02).

fraction study: a = 8.6475(1) Å, c = 3.8594(1) Å.

First, calculations were carried out with a composition corresponding to a non-oxygen-deficient material. The starting positions of the different atoms were those obtained from the X-ray study: the large cations Ba^{2+} and La^{3+} were first located on the 1(d) and 4(k) sites, respectively, taking into account the A–O distances and their molar ratio, Ba/La = 1/4; the copper ions were distributed over the 1(a) and 4(j) sites and the 15 oxygen atoms on the 1(b), 2(e), 4(j), and 4(k) sites. Atomic parameters and occupancy factors of oxygen sites were refined successively. At this point, the occupancy factor of the 2(e) site was found to be very low and localization of the oxygen vacancies in these positions was expected. Then, 13 oxygen atoms were distributed over the 1(b), 4(j), and 4(k) sites and the excess of oxygen, noted O(2), with respect to the formulation $BaLa_4Cu_5O_{13}$, in the 2(e) positions. New refinements of atomic parameters and thermal parameters were carried out. Then occupancy of 2(e) sites by oxygen atoms $O_{(2)}$ whose B factor was fixed at 1 Å^2 was refined leading to a δ value of 0.12 ± 0.04, very close to the one obtained by chemical analysis. After final refinement the discrepancy factor calculated on the intensities was lowered to R_I = 0.044 (R_P = 0.103; R_e = 0.048; R_{wp} = 0.115) for the different variables given in Table I. During the refinement, anisotropic agitation was introduced for barium atoms and for one of the oxygen atoms O(1) owing to the large standard deviation observed for the isotropic factors of these atoms.

Calculations carried out with a statistical distribution of barium and lanthanum over the 1(d) and 4(k) sites led to a significant increase of the discrepancy factor.

These results support the first model. Nevertheless, the possibility of existence of an oxygen-deficient $BaLa_4Cu_5O_{14-x}$ structure cannot be rejected: it would be characterized by a monoclinic symmetry; such a

TABLE II

INTERATOMIC *M*–O DISTANCES: NEUTRON DIFFRACTION

M–O		Distance (Å)
Cu(1)–O(1)	× 2	1.930(1)
Cu(1)–O(4)	× 4	2.039(6)
Cu(2)–O(2)	× 1	1.656(4)
Cu(2)–O(3)	× 1	2.272(11)
Cu(2)–O'(3)	× 1	1.880(11)
Cu(2)–O(4)	× 1	1.875(11)
Cu(2)–O(5)	× 2	1.935(1)
Ba–O(3)	× 8	2.930(5)
Ba–O(5)	× 4	3.063(5)
La–O(1)	× 1	2.647(4)
La–O(2)	× 2	2.938(3)
La–O(3)	× 2	2.489(7)
La–O(4)	× 2	2.811(8)
La–O'(4)	× 2	2.581(7)
La–O(5)	× 1	2.720(10)
La–O'(5)	× 1	2.653(9)
La–O''(5)	× 1	2.710(10)

pseudotetragonal structure which could involve a drastic increase of the variables cannot be seriously tested by powder diffraction. However, the consideration of the final structure is in good agreement with the $BaLa_4Cu_5O_{13}$ structure. The Cu–O distances (Table II) ranging from 1.93 to 2.039 Å in the CuO_6 octahedra and from 1.88 to 2.27 Å in the CuO_5 pyramids are close to those usually observed in the copper oxides. The geometry of the CuO_5 pyramid, with four average Cu–O distances (1.88 to 1.93 Å) and one longer distance (2.27 Å) which is trans to the oxygen vacancy, has often been observed in square pyramids: it results from unequal occupancy of the d_{z^2} and $d_{x^2-y^2}$ orbitals.

The very short Cu(2)–O(2) distance (1.65 Å) suggests that the additional oxygen (O(2)) is not, in fact, distributed statistically in the hexagonal tunnels of the $BaLa_4Cu_5O_{13}$ structure (Fig. 2a) but can be due either to the existence of $BaLa_4Cu_5O_{14}$ domains or to the presence of other defects richer in oxygen in the matrix of different crystals. The distortion of the hexagonal tunnels with respect to the ideal $BaLa_4Cu_5O_{13}$ structure is in agreement with this point of view: the O(3)–O(4)–O(4) angle close to 70°, instead of 90° in the idealized model, and the short O(5)–O(5) distances, close to 3 Å (instead of 3.8 Å), which correspond to the displacement of the O(5) atoms toward the center of the tunnels, are easily explained by the fact that the O(2) sites are vacant.

High-Resolution Electron Microscopy Study

The large majority of the microcrystals, observed with a [001] incident beam direction, exhibit the contrast shown in Fig. 3. The main contrast features concern the rows of bright dots separated by lines of darkness. It is worth noting that a drastic variation of the spacing and the size of the white spots was observed by changing the focus value and with the thickness of the crystals. Thus, it was necessary to perform image calculations in order to interpret the experimental images.

Simulations were carried out using the atomic positions obtained from the neutron diffraction study and, for the ideal composition $BaLa_4Cu_5O_{13}$, thicknesses 12 Å $\leq t \leq$ 100 Å. As an example, a part of a focus series for experimental and calculated images (for a crystal thickness of 30.9 Å) is shown in Fig. 4. Thus, for $\Delta f \sim 500$ Å the small white dots spaced ~2.8 Å apart correspond to the positions of the oxygen atoms and the largest ones (two per cell) to the oxygen vacancies, whereas for a focus value $\Delta f \sim 800$ Å the positions of the heavy atoms appear as white dots: the largest ones correspond to the Ba ions surrounded by four pyramids and the small ones to the lanthanum in the hexagonal tunnels.

The comparison of the calculated and experimental images shows clearly that the crystals are homogeneous and confirms

FIG. 3. Typical image obtained from our sample with the electron beam parallel to [001].

that the structure belongs to the $BaLa_4Cu_5O_{13}$ type. This homogeneity of the crystals, and these computer simulations, allows the possibility of the existence of $BaLa_4Cu_5O_{14}$ domains in such crystals to be ruled out. Simulations performed on the basis of this latter hypothesis show, indeed, calculated images rather different from the observed ones. These results and those obtained by neutron diffraction, and especially those from consideration of interatomic distances, are in good agreement with the stoichiometric structure $BaLa_4Cu_5O_{13}$ for a great number of crystals.

From this study, it appears that the deviation from the stoichiometry $BaLa_4Cu_5O_{13}$ would not be due to a random distribution of the additional oxygen in the hexagonal tunnels but should correspond to the presence of irregular crystals or of crystals characterized by a distorted framework with respect to $BaLa_4Cu_5O_{13}$ in order to accommodate the oxygen excess. The electron diffraction study confirms this point of view: it reveals the presence of crystals characterized by a double $BaLa_4Cu_5O_{13}$-type cell with $a_p\sqrt{10} \times a_p\sqrt{10} \times a_p$. Such a pattern is shown in Fig. 5; the intensity of the superstructure reflections varies from one crystal to the other. Two hypotheses can be considered to explain this phenomenon; both are related to an excess of oxygen with regard to the stoichiometric $BaLa_4Cu_5O_{13}$ oxide. The first one corresponds to

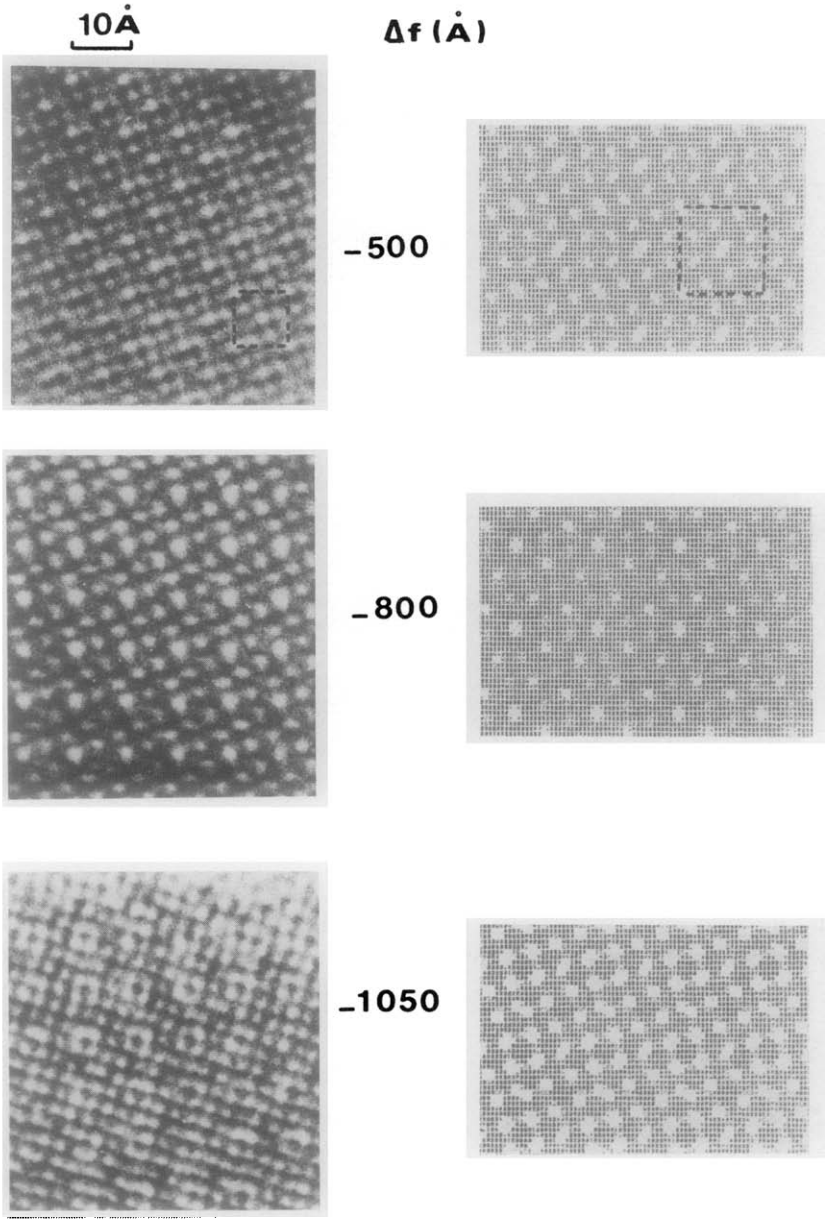

FIG. 4. High-resolution images. Part of the experimental and calculated focus series (t = 30.9 Å) [001].

a formulation $BaLa_4Cu_5O_{13.5}$, with three oxygen vacancies per double cell; the idealized drawing of such a model is shown in Fig. 6. It is built up from four octahedra and six pyramids. As in the $BaLa_4Cu_5O_{13}$ structure, hexagonal tunnels exhibit alternate orientations; it could be considered an intergrowth of slabs of $BaLa_4Cu_5O_{14}$ and $BaLa_4Cu_5O_{13}$ parallel to $\langle 130 \rangle_p$, i.e., the a axis of the double cell. The second one corre-

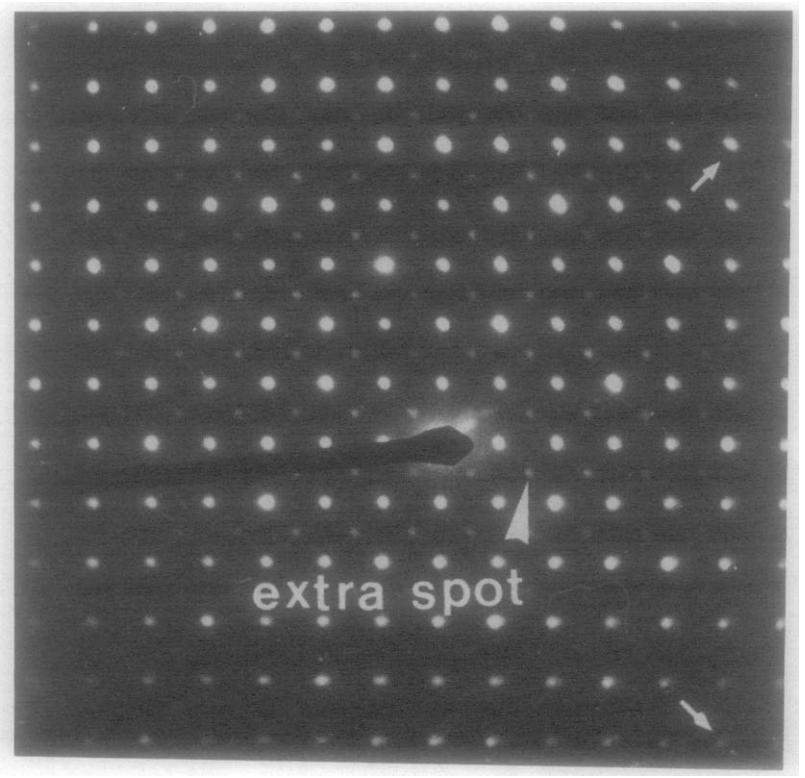

FIG. 5. Electron diffraction pattern with [001] exhibiting extra spots corresponding to a double cell: $a_p\sqrt{10} \times a_p\sqrt{10}$.

sponds to a simple distortion of the $a_p\sqrt{5} \times a_p\sqrt{5}$ cell, due to a small excess of oxygen randomly located in the hexagonal tunnels;

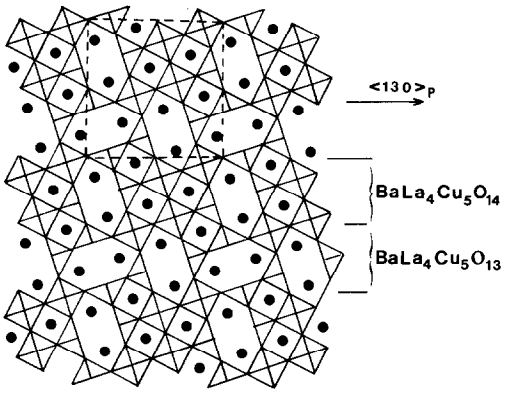

FIG. 6. Idealized drawing of a hypothetical model corresponding to three oxygen vacancies per cell ($a_p\sqrt{10} \times a_p\sqrt{10} \times a_p$).

this distortion results from the introduction of additional oxygen in the hexagonal tunnels of the $BaLa_4Cu_5O_{13}$ structure, involving displacement of the atoms surrounding the 2(*c*) sites and especially of the O(5) atoms. It must also be pointed out that such superstructure spots induce generally a monoclinic distortion of the tetragonal lattice (Fig. 5). Unfortunately no high-resolution image could be obtained from those crystals; a modification of the electron diffraction pattern was indeed observed after exposure to the electron beam. All the extra spots disappeared and the contrast was then similar to the one observed for the $a_p\sqrt{5} \times a_p\sqrt{5}$ cell. This phenomenon suggests a loss of oxygen and is consistent with both hypotheses but does not allow a choice between a new ordering scheme (with $\delta = 0.5$) and a random distribution

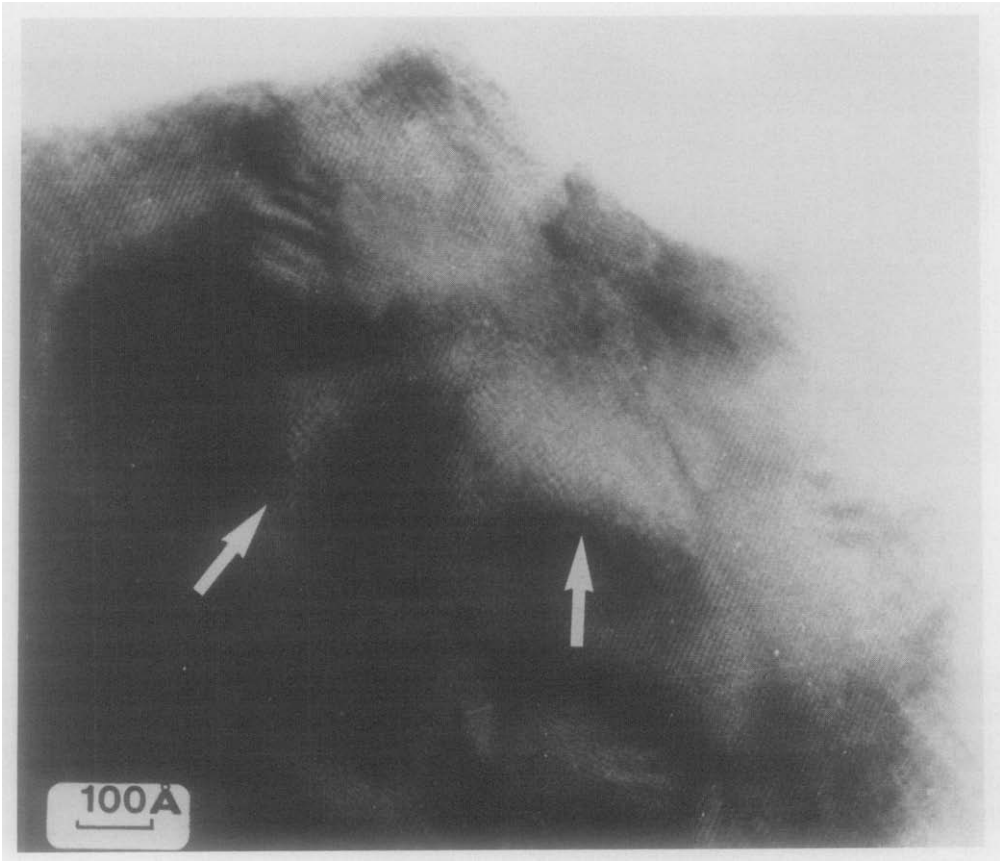

FIG. 7. Image of a crystal characterized by the presence of microdomains corresponding to modulations of the intensity and loss of the periodicity (white arrows).

(with unknown δ) of the additional oxygen. However, the uneven contrast observed in small areas of some microcrystals, such as modulations of the intensity and loss of periodicity in the form of microdomains (Fig. 7), could be interpreted in terms of local variations of the arrangements of the anionic vacancies.

A small number of crystals exhibit an electron diffraction pattern more closely related to the parent perovskite subcell but characterized by a monoclinic distortion. The micrography corresponding to such a crystal is shown in Fig. 8a; the regions labeled 1 and 3 of the crystal are "pseudocubic" (a_p) and region 2 is tetragonal ($a_p\sqrt{5} \times a_p\sqrt{5}$). The different parts are slightly misaligned (Fig. 8b). Such pseudocubic domains have been previously observed in the oxygen-deficient oxides $Sr_2Mn_2O_5$ (*9, 10*) and $Sr_2Mn_{2-x}M'_xO_5$ (M = Ti, Fe) (*16, 17*), built up from MnO_5 square pyramids, they have grown coherently in the matrix in the form of more or less small microdomains. It was shown that they could correspond either to AMO_3 or to $AMO_{2.5}$ formulations (with an aleatory arrangement of the deficient $AMO_{2.5}$ layers) or to an intermediate oxygen content.

In conclusion, the occurrence of such periodicity appearing in the form of single microcrystals, or of misaligned parts of one crystal, suggests that the introduction of oxygen in the $BaLa_4Cu_5O_{13}$ structure in-

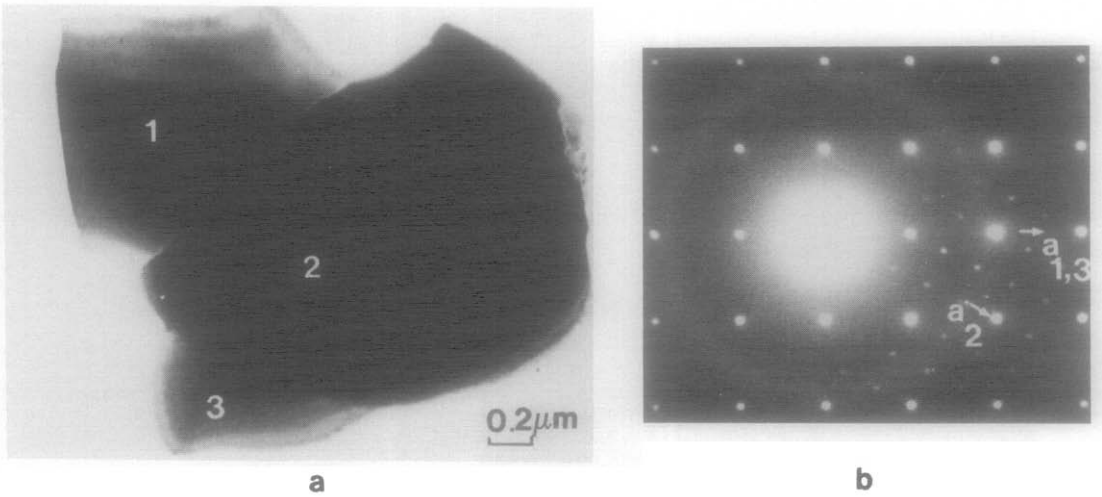

FIG. 8. (a) Low-resolution image and (b) electron diffraction pattern of a microcrystal exhibiting areas with a pseudocubic cell (zones 1 and 3) and tetragonal one (zone 2). It should be noted that the different areas are slightly misaligned.

duced a distortion of the framework and explains the oxygen nonstoichiometry in the oxide $BaLa_4Cu_5O_{13+\delta}$. In this respect, the study of the controlled oxidation of this oxygen-deficient perovskite will be necessary in order to understand the relationships between the structure and the electron transport properties of these metallic oxides.

References

1. N. NGUYEN, L. ER-RAKHO, C. MICHEL, J. CHOISNET, AND B. RAVEAU, *Mater. Res. Bull.* **15,** 891 (1980).
2. L. ER-RAKHO, C. MICHEL, J. PROVOST, AND B. RAVEAU, *J. Solid State Chem.* **37,** 151 (1981).
3. N. NGUYEN, J. CHOISNET, M. HERVIEU, AND B. RAVEAU, *J. Solid State Chem.* **39,** 120 (1981).
4. K. R. POEPPELMEIER, M. E. LEONOWICZ, AND J. M. LONGO, *J. Solid State Chem.* **44,** 89 (1982).
5. K. R. POEPPELMEIER, M. E. LEONOWICZ, J. C. SCANLON, J. M. LONGO, AND W. B. YELON, *J. Solid State Chem.* **45,** 71 (1982).
6. A. RELLER, D. A. JEFFERSON, J. M. THOMAS, R. A. BEYERLEIN, AND K. R. POEPPELMEIER, *J. Chem. Soc. Chem. Commun.*, p. 1378 (1982).
7. A. RELLER, J. M. THOMAS, D. A. JEFFERSON, AND M. K. UPPAL, *J. Phys. Chem.* **87,** 313 (1983).
8. A. RELLER, J. M. THOMAS, D. A. JEFFERSON, AND M. K. UPPAL, *Proc. R. Soc. London A* **394,** 223 (1984).
9. V. CAIGNAERT, N. NGUYEN, M. HERVIEU, AND B. RAVEAU, *Mater. Res. Bull.* **20,** 479 (1985).
10. V. CAIGNAERT, M. HERVIEU, N. NGUYEN, AND B. RAVEAU, *J. Solid State Chem.* **61,** 1986.
11. C. MICHEL, L. ER-RAKHO, AND B. RAVEAU, *Mater. Res. Bull.* **20,** 667 (1985).
12. H. M. RIETVELD, *J. Appl. Crystallogr.*, **2,** 65 (1969).
13. A. W. HEWAT, Harwell Report AERE-R7350 (1973).
14. L. KOESTER AND H. RAUGH, "Summary of Neutron Scattering Lengths," IAEA Contract 2517/RB (1981).
15. A. J. SKARNULIS, E. SUMMERVILLE, AND L. EYRING, *J. Solid State Chem.* **23,** 59 (1978).
16. V. CAIGNAERT, M. HERVIEU, J. M. GRENECHE, AND B. RAVEAU, *Chem. Scripta,* in press.
17. V. CAIGNAERT, M. HERVIEU, AND B. RAVEAU, *J. Nat. Res. Bull.* **21** (10) 1147 (1986).